A Millimeter Wave Multi-beam Transparent Transmitarray Antenna at Ka-band

Guang Liu, Mohammad Reza Dehghani Kodnoeih, Kien T. Pham, Eduardo Motta Cruz, D. Gonzalez-Ovejero, Ronan Sauleau

A Millimeter Wave Multi-beam Transparent Transmitarray Antenna at Ka-band

Guang Liu, Mohammad Reza Dehghani Kodnoeih, *Student Member, IEEE*, Kien T. Pham, *Member, IEEE*, Eduardo Motta Cruz, David Gonz ález-Ovejero, *SeniorMember, IEEE*, and Ronan Sauleau, *Fellow, IEEE*

***Abstract*—This letter presents a transmitarray antenna (TA) in the 27.5-29.5 GHz frequency band. The proposed TA is optically transparent and offers the possibility of steering the beam in the H-plane from -30 °to 30 °. One can achieve these properties using a novel unit-cell, composed of meshed double-circle rings printed on polymethylmethacrylate (PMMA) substrates, a plastic material transparent to visible light. This unit-cell provides a phase-shift of 300 °for an insertion loss lower than 1 dB at 28.5 GHz. In turn, the TA sources consist of 2×2-element arrays of aperture-coupled stacked patch antennas. The choice of a patch array over a horn array allows one to reduce the total profile and weight of the TA. We have fabricated and tested a transparent TA with a diameter of 9.9 wavelengths at 28.5 GHz, yielding a broadside gain of 25 dBi and -1 dB gain bandwidth of 1.8 GHz, off-axis 30 °beam presents a peak gain of 21.5 dBi and -1 dB gain bandwidth of 1.4 GHz. The measured results are in good agreement with the simulated ones all over the frequency band of interest.**

***Index Terms*— transmitarray antennas, millimeter waves, multi-beam antenna, aperture-coupled stacked patch array, transparent antennas.**

I. Introduction

RECENTLY, there has been a high demand for millimeter wave high-gain antennas with wide bandwidths and beam steering capabilities to achieve the high data rates targeted by future 5G communications [1]. One of the key aspects in 5G networks will be the deployment of a large number of small cells in heterogeneous networks. Therefore, optically transparent and planar antennas are attractive to minimize the visual impact of such deployments. This antenna topology could be widely integrated on windows of buildings, windshields of vehicles and solar panels, without obstructing the sight and absorbing energy from sun light [2]. They are also promising candidates for communication systems in smart street furniture [3].

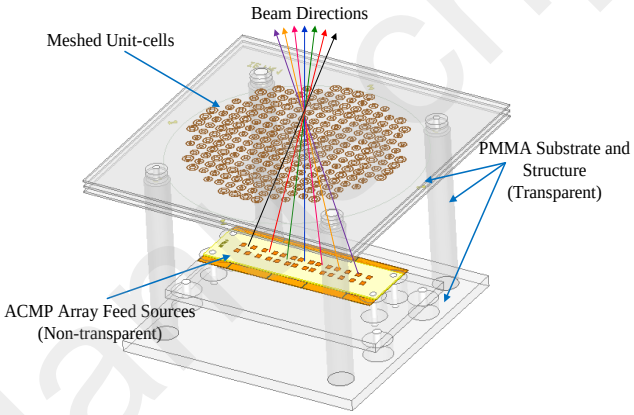

Fig. 1 3D view of the TA, where the TA aperture is transparent.

In this context transmitarray antennas (TA) [4],[5] can provide high gains and good aperture efficiencies over large bandwidths, while avoiding blockage from the feed (as opposed to reflectarrays), and the losses in the feeding network (as opposed to antenna arrays). Moreover, they are flat and one can fabricate them at low cost by standard printed circuit technology. However, low visual impact combined to beam steering has not yet been addressed. An effective solution to achieve beam steering would be to displace mechanically the source on the focal plane [6], at the cost of increasing the weight and limiting the beam steering speed to that of the mechanical motor platform.

This paper deals with the two aforementioned challenges with a transparent TA (TTA) able to switch the beam in the H-plane at Ka band. Fig. 1 shows the structure of the proposed TTA. We have selected polymethylmethacrylate (PMMA) as substrate for the TA, due to its good transparency in the visible range (> 92%), lightweight, low cost and mechanical robustness. In turn, the TA unit-cell consists of meshed double circle rings to prevent a degradation of the transparency, while preserving good transmission characteristics at Ka band. The TA sources consist of 2×2-element arrays of aperture-coupled microstrip patch (ACMP) antennas. The spacing between elements is optimized in order to compensate for the mutual coupling effects in the pattern, which should present rotational symmetry and an edge illumination of -11 dB to have a com-

Manuscript received September 4th, 2018, revised January 15th, 2019.

G. Liu was with IETR, UMR CNRS 6164, Universit é de Nantes, Polytech Nantes. He is now with CAS Key Laboratory of Microwave Remote Sensing, National Space Science Center, Chinese Academy of Sciences, Beijing 100190, China (e-mail: guang.liu@univ-nantes.fr, liuguang@mirslab.cn).

K. T. Pham was with IETR, UMR CNRS 6164, Universit é de Rennes 1, 35042 Rennes, France. He is now with International University, VNU-HCM, Ho Chi Minh City, Vietnam (e-mail: trung-kien.pham.1@univ-rennes1.fr, ptkien@hcmiu.edu.vn).

M. R. Dehghani Kodnoeih is with IETR, UMR CNRS 6164, Universit é de Nantes, Polytech Nantes, 44306 Nantes, France, and with Radio Frequency Systems, 44570 Trignac, France (e-mail: mohammad.dehghani@univ-nantes.fr).

E. Motta Cruz is with IETR, UMR CNRS 6164, Universit é de Nantes, Polytech Nantes, Rue Christian Pauc, 44306 Nantes, France (e-mail: eduardo.mottacruz@univ -nantes.fr).

D. Gonz ález-Ovejero, and R. Sauleau are with IETR, UMR CNRS 6164, Universit é de Rennes 1, 35042 Rennes, France (e-mails: david.gonzalez-ovejero, ronan.sauleau}@univ-rennes1.fr).

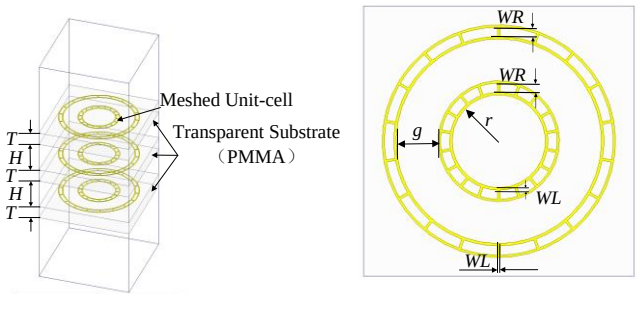

(a) (b)

Fig. 2 Meshed double circle rings unit-cell, (a) perspective view, (b) top view.

promise between spillover loss and illumination efficiency. Then, seven ACMP arrays placed in the focal plane provide seven different orientations for the beam. One could use GaAs MMIC switches to activate alternatively these arrays and realize beam steering from -30 °to 30 °with 10 °step, e.g. [7], [8].

This paper is organized as follows. Section II describes the meshed double circle rings unit-cell, presents the design of the ACMP antenna array used as source, and shows the simulation results of TTA. Section III reports the experimental validation of the TTA prototype. Conclusions are drawn in Section IV.

II. Transparent Transmitarray Antenna and Design of The Feed Array

A. *Meshed Double Circle Rings Unit-cell*

The TA unit-cell is designed at f_0 = 28.5 GHz, which is the center frequency of the objective frequency band. The size of the unit-cell is $0.55\lambda_0 \times 0.55\lambda_0$, where λ_0 is the free-space wavelength at f_0. The unit-cell, shown in Fig. 2, consists of three metallization layers with two concentric meshed rings per layer. Each meshed ring is composed of two concentric circular lines and 18 radial lines which connect the inner and outer circular lines, as depicted in Fig. 2(b). We set the width of the metallic lines in the meshed unit-cell to *WL*=0.5mm due to the limitations of standard PCB printing technology, and to reduce the ohmic losses (higher for smaller line widths [9]). Doing so, one obtains the best compromise between transparency of the printed PMMA panels and transmission performance. The spacing between the two circular lines in a meshed ring is *WR* = 0.2 mm, and the angle between two adjacent radial lines is 20 °. In turn, the spacing between the two meshed rings is g = 0.9 mm. One can tune the phase of the transmission coefficient by varying the inner radius r of the smallest circular line in the inner ring. The metallic patterns are printed on three identical PMMA substrates (ε_r = 2.3, tanδ = 0.01), as shown in Fig. 2(a), the substrate thickness is T = 0.8mm. The spacing between two layers is $T+H = \lambda_0/4$ = 2.63 mm.

Fig. 3 shows the magnitude and phase response of the meshed unit-cell transmission coefficient under various angles of incidence at 28.5 GHz. Fig. 3 also illustrates how the phase response of the unit-cell can be controlled by varying r. We have obtained these simulated results by using periodic boundary conditions and Floquet ports in Ansys HFSS v.18.1. The obtained results indicate that one can achieve a phase range

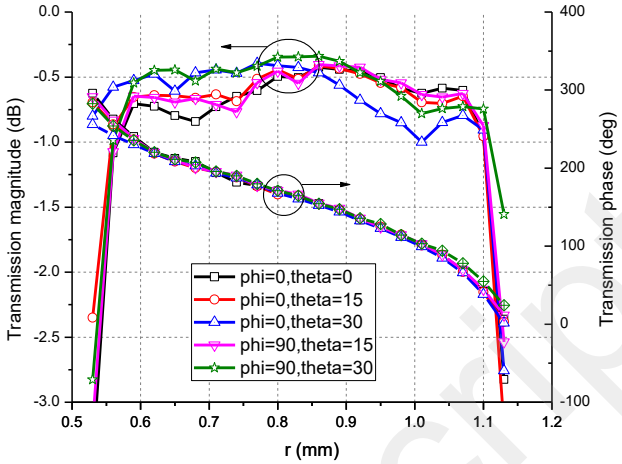

Fig. 3 Simulated magnitude and phase response of the meshed unit-cell at 28.5 GHz.

of 290 °with a transmission loss lower than 3dB. The insertion loss of the meshed unit-cell is smaller than 1 dB for most of the values of r and for oblique angles of incidence of up to 30 °, both for TE- and TM-polarized waves. Moreover, the phase curves under normal and oblique incidences present a good linearity and are almost coincident, with phase variations smaller than 28 °. This behavior indicates the low sensitivity of the unit-cell to oblique incidence angles. The low transmission loss and the excellent phase stability for oblique incidence confirm the good transmission performance of the proposed transparent unit-cell. The comparison between the meshed and non-meshed unit-cell results [10], indicate very good agreement of the transmission performance between these two kinds of unit-cells.

B. *Design of the Focal Plane ACMP Arrays*

The focal sources consist of 2 ×2 arrays of ACMP antennas. This choice allows one to reduce the overall weight and bulkiness of the transparent TA and to be compatible with RF circuits for electronic beam steering purposes. The right inset in Fig. 4 shows an exploded view of the ACMP array. The bottom substrate includes the feeding microstrip lines on the bottom side and the coupling slots on top. The main patches are printed on the middle substrate, and the parasitic ones on the top substrate. Table I provides the main dimensions of all these elements and the inter-element spacing of the array elements is 5.5 mm in both planes.

TABLE I. ACMP Array Design Dimensions

Main patch dimensions	2.6mm × 2.27mm	**Feed line width**	0.3 mm
Parasitic patch dimensions	2.6mm × 2.27mm	**Slot aperture**	1.65mm × 0.2mm
Bottom substrate thickness	0.13mm	**Intermediate substrate thickness**	0.13mm
Top substrate thickness	0.508mm	**Bonding layers thickness**	0.038mm

Fig. 4 presents the simulated normalized radiation pattern of the ACMP array. The 2 ×2 array offers a gain of 11.3 dBi and an illumination edge taper of around 11 dB in both planes (when

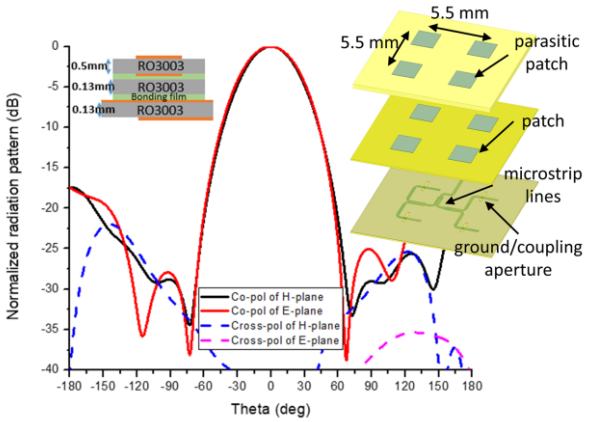

Fig. 4 Radiation pattern of the 2×2 ACMP antenna array computed at 28.5 GHz. The left inset shows the stacked substrates configuration, whereas the right one shows a perspective view of the ACMP antenna.

this focal array is centered), which allows one to minimize the TA spillover loss.

C. *Transparent Transmitarray Antenna Design*

The designed TA consists of a circular aperture with diameter $D = 9.9\lambda_0 = 104.4$ mm. The F/D ratio is 0.5, with F being the focal distance, and the phase correction function is obtained as in [11]. This choice of dimensions responds to the objective of obtaining a minimum gain of 22 dBi in the ±30 ° angular range. One can obtain the target angular coverage by the seven discrete beams associated to each ACMP array; such beams present an overlap level between adjacent beams better than 3 dB. To that end, the positions of the seven ACMP array are optimized and displaced from -30.1 mm to 30.1 mm along x-axis in the focal plane of the transparent TA. The off-axis feeds placed to the right of the central one are placed at 9.2 mm, 19 mm and 30.14 mm from the focal point. This geometry allows one to obtain beams pointing at -10 °, -20 ° and -30 °. The feeds on the left side are the symmetrical counterpart of those on the right. All the feeds are excited by the same power level. Fig. 5 shows the simulated gain curves versus frequency for the beams pointing at 0 °, -10 °, -20 ° and -30 °. The broadside beam presents a peak gain of 26.2 dBi and a -1 dB gain bandwidth of 8.1%, whereas the off-axis beam pointing at -30 ° presents a peak gain of 22.5 dBi and a -1 dB gain bandwidth of 8.8%.

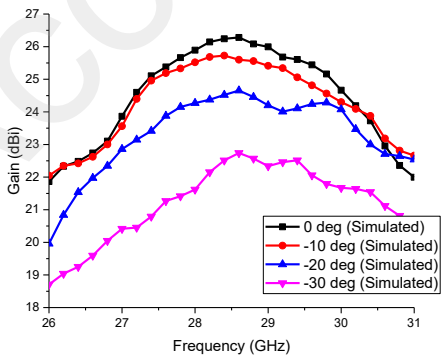

Fig. 5. Simulated gain versus frequency for the broadside and off-axis beams.

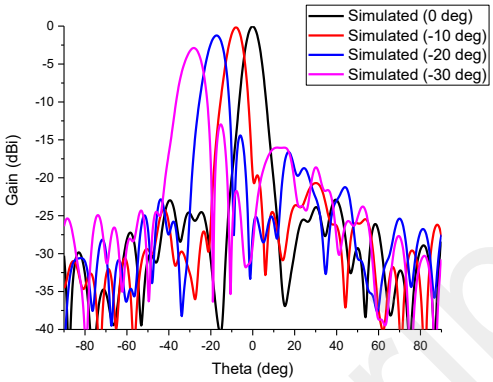

Fig. 6. Normalized simulated gain patterns for the broadside and off-axis beams of the transparent TA at 28.5 GHz

Fig. 6 shows the normalized simulated radiation patterns of the broadside and off-axis beams at 28.5 GHz. As the scanning angle increases from 0 ° to -30 °, the gain of beam decreases from 26.2 dBi to 22.5 dBi, and the side lobe level increases from -23 dB to -10 dB.

III. Experimental Results

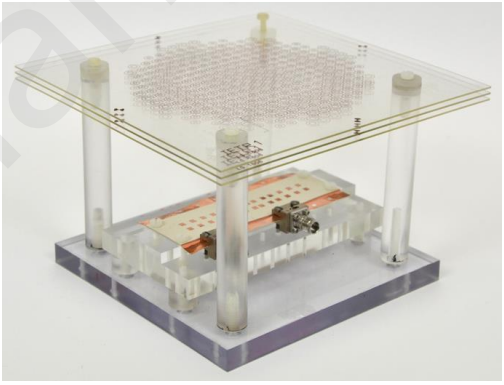

Fig. 7. Picture of the transparent TA prototype.

The transparent TA has been fabricated using standard photolithography on the PMMA substrates. Fig. 7 shows a picture of the fabricated TA prototype, with the three PMMA stacked using transparent plastic spacers. The alignment of the three PMMA substrates was carried out by drilling four holes

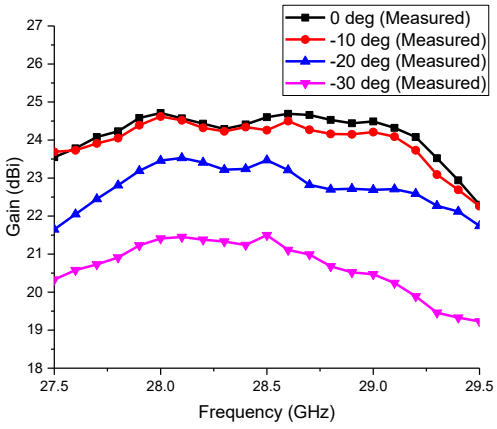

Fig. 8. Measured gain versus frequency for the broadside and off-axis beams.

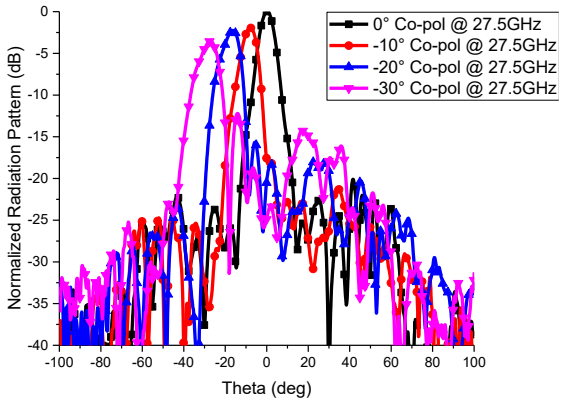

(a)

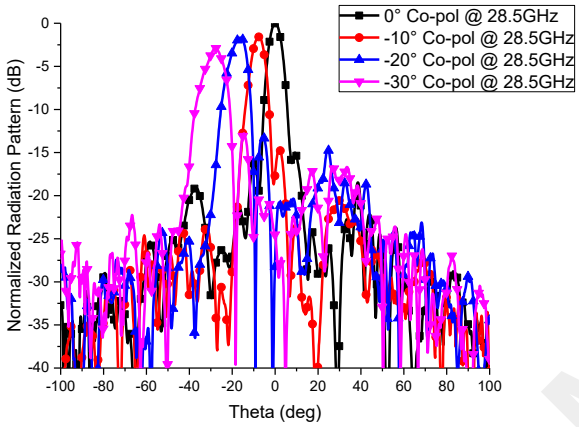

(b)

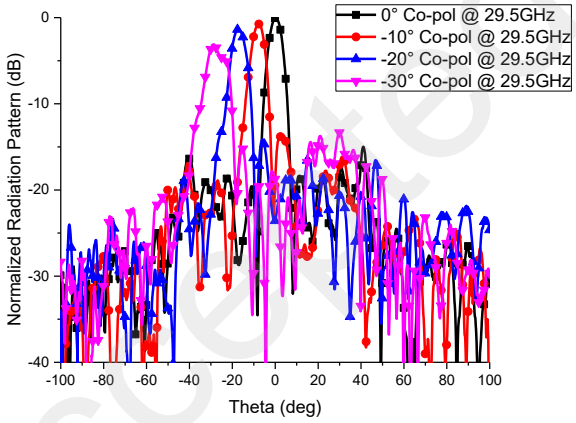

(c)

Fig. 9. Measured normalized radiation patterns of the broadside and off-axis beams in the H-plane at (a) 27.5 GHz, (b) 28.5 GHz, and (c) 29.5 GHz.

on each panel and using dowel pins in two of the supporting struts. The three layers were hold together using four plastic screws, one per strut. Appropriate 2.92mm end-launch connectors are used to excite the microstrip feeding networks of the 2×2 ACMP arrays, so one can carry out the measurement.

Fig. 8 shows the gain versus frequency curves for the broadside and off-axis beams. The measured broadside beam presents a peak gain of 25 dBi, which implies an aperture and

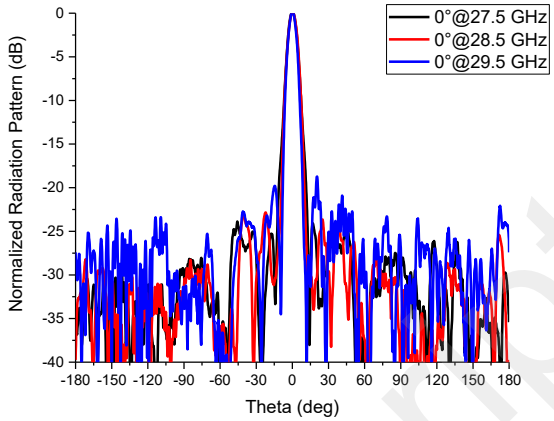

Fig. 10. Measured normalized gain patterns in the E-plane at 27.5, 28.5 and 29.5 GHz.

radiation efficiency of 32.3% and 75.9%, respectively, and a -1 dB gain bandwidth of 6.3%. On the other hand, the off-axis beam pointing at 30 °presents a peak gain of 21.5 dBi and a -1 dB gain bandwidth of 4.9%.

Fig. 9 represents the measured radiation patterns of the prototype in the H-plane at 27.5 GHz, 28.5 GHz and 29.5 GHz. The gain scan-loss for the -30 º off-axis beams at the lower frequency (27.5 GHz), the center frequency (28.5 GHz) and the upper frequency (29.5 GHz) are -3.6 dB, -2.9 dB, and -3.3 dB, respectively. The H-plane side-lobe levels are 12.4 dB below the maximum from 27.5 GHz to 29.5 GHz for all the off-axis beams. There are two main reasons for the differences between measured and simulated results. First, the actual tanδ of PMMA may be larger than 0.01, and the coaxial connector could introduce additional losses. Second, assembly tolerances of the TTA and the position error of the feeds bring into the differences between measured and simulated results.

In the E-plane, the main beams of the normalized radiation patterns at the center, lower and upper frequencies are almost coincident and symmetrical, as shown in Fig. 10. The E-plane side lobe levels are lower than -18.7 dB at the three frequency points.

IV. Conclusion

This paper shows the design of an optically transparent TA fed by seven 2×2-element aperture-coupled stacked patch antenna arrays. This structure presents a low profile and low weight, and allows one to control the beam direction by switching from one focal array to the next one. The meshed double-ring proposed as unit-cell presents a transmission behavior with low transmission loss and weak dependence to the angle of incidence at Ka-band. The simulation and measurement results show beam scanning in a wide angular range of ±30 °with a high gain (> 19.5 dBi) and low side lobe level (< -12.4 dB) between 27.5 GHz and 29.5 GHz.

This type of antenna with reduced visual impact could be attractive from 5G small-cells and smart street furniture. Future work will focus on reducing the scan loss and the side lobe level of the off-axis beams, and on the design of a fully electronically switchable focal array.

REFERENCES

[1] W. Hong, *et al*., "Multibeam antenna technologies for 5G wireless communications," *IEEE Trans. Antennas Propag.*, vol. 65, no. 12, pp. 6231-6249, Dec. 2017.

[2] C. Kocia and S. V. Hum, "Design of an optically transparent reflectarray for solar applications using Indium Tin Oxide," *IEEE Trans. Antennas Propag.*, vol. 64, no. 7, pp. 2884–2893, Jul. 2016.

[3] L. Manholm, J. Fridén, and B. E. Olsson, "Deployment considerations for 60 GHz backhaul using smart street furniture," *9th Eur. Conf. Antennas Propag. (EuCAP)*, Lisbon, Portugal, 2015.

[4] H. Kaouach, L. Dussopt, J. Lanteri, T. Koleck, and R. Sauleau, "Wideband low-loss linear and circular polarization transmit-arrays in V-band," *IEEE Trans. Antennas Propag.*, vol. 59, no. 7, pp. 2513-2523, Jul. 2011.

[5] C. Jouanlanne, *et al*., "Wideband linearly polarized transmitarray antenna for 60 GHz backhauling," *IEEE Trans. Antennas Propag.*, vol. 65, no. 3, pp. 1440-1445, Mar. 2017.

[6] K. Pham, *et al.*, "Design of wideband dual linearly polarized transmitarray antennas," *IEEE Trans. Antennas Propag.*, vol. 64, no. 5, pp. 2022-2026, May 2016.

[7] T. Potelon, *et al.*, "A low-profile broadband 32-slot continuous transverse stub array for backhaul applications in E-band," *IEEE Trans. Antennas Propag.*, vol. 65, no. 12, pp. 6307-6316, Dec. 2017.

[8] F. Foglia Manzillo, *et al*., "A multilayer LTCC solution for integrating 5G access point antenna modules," *IEEE Trans. Microw. Theory Tech.*, vol. 64, no. 7, pp. 2272-2283, Jul. 2016.

[9] J. Hautcoeur, F. Colombel, X. Castel, M. Himdi, and E. M. Cruz, "Optically transparent monopole antenna with high radiation efficiency manufactured with silver grid layer (AgGL)," *Electron. Lett.*, vol. 45, no. 20, pp. 1014-1016, 24 Sep. 2009.

[10] G. Liu, K. Pham, E. Motta Cruz, D. Gonzâlez Ovejero, and R. Sauleau, "A millimeter wave transparent transmitarray antenna using meshed double circle rings elements", *2018 Eur. Conf. Antennas Propag.*, London, UK, 9-13 Apr., 2018.

[11] G. Liu, H. J. Wang, J. S. Jiang, F. Xue, and M. Yi, "A high-efficiency transmitarray antenna using double split ring slot elements," *IEEE Antennas Wireless Propag. Lett*., vol. 14, pp. 1415-1418, 2015.